ARTICLES

Multimodal fast optical interrogation of neural circuitry

Feng Zhang[1], Li-Ping Wang[1], Martin Brauner[2], Jana F. Liewald[2], Kenneth Kay[1], Natalie Watzke[4], Phillip G. Wood[4], Ernst Bamberg[3,4], Georg Nagel[4,5], Alexander Gottschalk[2] & Karl Deisseroth[1]

Our understanding of the cellular implementation of systems-level neural processes like action, thought and emotion has been limited by the availability of tools to interrogate specific classes of neural cells within intact, living brain tissue. Here we identify and develop an archaeal light-driven chloride pump (NpHR) from *Natronomonas pharaonis* for temporally precise optical inhibition of neural activity. NpHR allows either knockout of single action potentials, or sustained blockade of spiking. NpHR is compatible with ChR2, the previous optical excitation technology we have described, in that the two opposing probes operate at similar light powers but with well-separated action spectra. NpHR, like ChR2, functions in mammals without exogenous cofactors, and the two probes can be integrated with calcium imaging in mammalian brain tissue for bidirectional optical modulation and readout of neural activity. Likewise, NpHR and ChR2 can be targeted together to *Caenorhabditis elegans* muscle and cholinergic motor neurons to control locomotion bidirectionally. NpHR and ChR2 form a complete system for multimodal, high-speed, genetically targeted, all-optical interrogation of living neural circuits.

To enable precise perturbation of living circuits, we recently developed an optogenetic[1] technology for genetically targeted, millisecond-timescale optical excitation of neurons[2,3] by employing an algal protein, channelrhodopsin-2 (ChR2)[4], which functions in many cell types[2–9]. However, because ChR2 can only test sufficiency of spike patterns in circuit or behavioural responses and cannot inhibit native spiking, testing the necessity or physiological function of targeted cells remains difficult. The ideal solution would be to complement ChR2 with a hypothetical light-activated hyperpolarizing agent, to permit excitation or inhibition using two light wavelengths while maintaining high temporal precision and genetic targeting. Several state-of-the-art methods[5,10–19] have been developed to kill or inactivate neurons, but none offers the necessary millisecond-precision, rapid reversibility and spectral compatibility for simultaneous use with fast, genetically based, photostimulation techniques such as ChR2.

Finding an optically compatible inhibitor

Our finding that ChR2 could depolarize neurons fast enough to drive precisely timed light-evoked spikes[2] motivated us to search for a complementary high-speed hyperpolarizing agent, to optically silence individual action potentials. ChR2 is highly homologous to ChR1 (ref. 20) and both are homologous to bacteriorhodopsin[4] and the light-driven chloride pumping halorhodopsins[21]. We predicted that the halorhodopsins could be used to optically inhibit neural activity, and we explored halorhodopsins from two strains of archaea, *Halobacterium salinarum* (HsHR) and *Natronomonas pharaonis* (NpHR). We initially characterized the halorhodopsins using *Xenopus laevis* oocytes (see Supplementary Methods for details). Illumination of HsHR- or NpHR-expressing oocytes led to rapid outward currents (Supplementary Fig. 1a). Both HsHR and NpHR have excitation maxima near 580 nm[22,23] (Fig. 1a; the action spectrum of NpHR was measured here in *Xenopus* oocytes using a xenon short arc lamp and narrow-bandwidth 20 nm filters), which, importantly, is red-shifted from the known ChR2 maximum of ~460 nm[4]. This spectral separation indicated to us that ChR2 and a halorhodopsin could be activated independently or in synchrony to effect bidirectional optical modulation of membrane potential.

The dependence of pump current on the extracellular Cl^- concentration for both halorhodopsins was assayed using whole-cell recording. HsHR was found to have a lower extracellular Cl^- affinity than NpHR ($K_{M,NpHR} = 16$ mM, Fig. 1b; $K_{M,HsHR} = 32$ mM) and measured currents showed rapid rundown at low extracellular Cl^- concentrations (Supplementary Fig. 1b), which did not fully recover in darkness. Halorhodopsin pumps are expected to have a very low affinity for Cl^- on the cytoplasmic side, where Cl^- ions are released, because halorhodopsin-mediated chloride pumping can achieve molar concentrations of cytoplasmic Cl^-. We found that the pump currents exhibited more or less linear voltage dependence, and Cl^- current was robust for both halorhodopsins across all physiological voltage regimes (for NpHR see Supplementary Fig. 1c). On the basis of NpHR's higher extracellular Cl^- affinity and stability, we chose to apply NpHR to neurons.

We introduced a mammalian codon-optimized *NpHR* gene fused with enhanced yellow fluorescent protein (*NpHR–EYFP*) into cultured rat hippocampal CA3/CA1 neurons using lentiviruses carrying the ubiquitous *EF1α* promoter (*EF1α-NpHR–EYFP*). Cells expressing NpHR–EYFP maintained robust expression (Fig. 1c) for weeks after infection. In voltage-clamp experiments, illumination of NpHR–EYFP cells with yellow light (bandwidth 573–613 nm using a Semrock filter FF01-593/40-25 and 300 W xenon lamp) induced rapid outward currents (Fig. 1d, upper panel) with a peak level of 43.8 ± 25.9 pA and a steady-state level of 36.4 ± 24.4 pA (mean ± s.d. reported throughout this paper, unless otherwise stated, $n = 15$; Fig. 1e). The relatively small difference between the peak and steady-state currents is indicative of rare deprotonation of the NpHR Schiff base during the pump cycle[22]. The rise time from light onset to 50% of the peak current was consistent across cells

[1]Department of Bioengineering, Stanford University, Stanford, California 94305, USA. [2]Institute of Biochemistry, and [3]Institute of Biophysical Chemistry, Department of Biochemistry, Chemistry and Pharmacy, Johann Wolfgang Goethe-University, Frankfurt Biocenter N220, Max-von-Laue Straβe 9, D-60438 Frankfurt, Germany. [4]Max-Planck-Institute of Biophysics, Max-von-Laue-Straβe 3, D-60438 Frankfurt am Main, Germany. [5]University Wuerzburg, Botanik I, Julius-von-Sachs-Platz 2, D-97082 Wuerzburg, Germany.

(6.0 ± 1.0 ms; Fig. 1f) with rise and decay time constants of $\tau_{on} = 6.1 \pm 2.1$ ms and $\tau_{off} = 6.9 \pm 2.2$ ms, respectively. Light-evoked responses were never seen in cells expressing EYFP alone (data not shown). In current-clamp experiments, NpHR–EYFP neurons exhibited light-evoked hyperpolarization (Fig. 1d; lower panel) with an average peak of 14.7 ± 6.9 mV and a steady-state of 12.1 ± 6.6 mV (Fig. 1g). The delay from light onset to 50% of hyperpolarization peak was 26.0 ± 8.6 ms (Fig. 1f), and the rise and decay time constants were $\tau_{on} = 35.6 \pm 15.1$ ms and $\tau_{off} = 40.5 \pm 25.3$ ms, respectively. To test whether NpHR-mediated hyperpolarization could inhibit neuronal firing, we injected current-clamped neurons with a 200 pA current step for 2 s to evoke robust spike firing; concurrent light delivery abolished the evoked activity (Fig. 1h). Therefore, NpHR can indeed serve as an optical inhibitor of neuronal activity.

We next verified that NpHR functions in an unperturbed intracellular environment. We co-expressed NpHR–EYFP and ChR2 tagged with a red fluorescent protein variant (ChR2–mCherry) in cultured hippocampal neurons (Fig. 2a), and we probed NpHR function using cell-attached recordings with ChR2 photostimulation to drive reliable spike trains. Indeed, whereas trains of blue light pulses were able to evoke action potentials through the activation of ChR2, concomitant yellow light illumination abolished spike firing in both cell-attached and subsequent whole-cell recoding modes (Fig. 2b). After achieving the whole-cell configuration, voltage-clamp recording showed that independent exposure to yellow or blue light led to outward or inward photocurrents, respectively (Fig. 2c). This further confirms that ChR2 and NpHR can be combined to achieve bidirectional, independently addressable modulation of membrane potential in the same neuron. In addition, we found that NpHR inhibitory function does not require a specific pipette chloride concentration under these recording conditions, because NpHR-mediated inhibition is robust across a range of relevant whole-cell pipette chloride concentrations (4–25 mM) and physiologically negative resting potentials (Supplementary Fig. 2)—as expected from the fact that NpHR has evolved to deliver chloride ions to molar levels in the archaeal intracellular milieu.

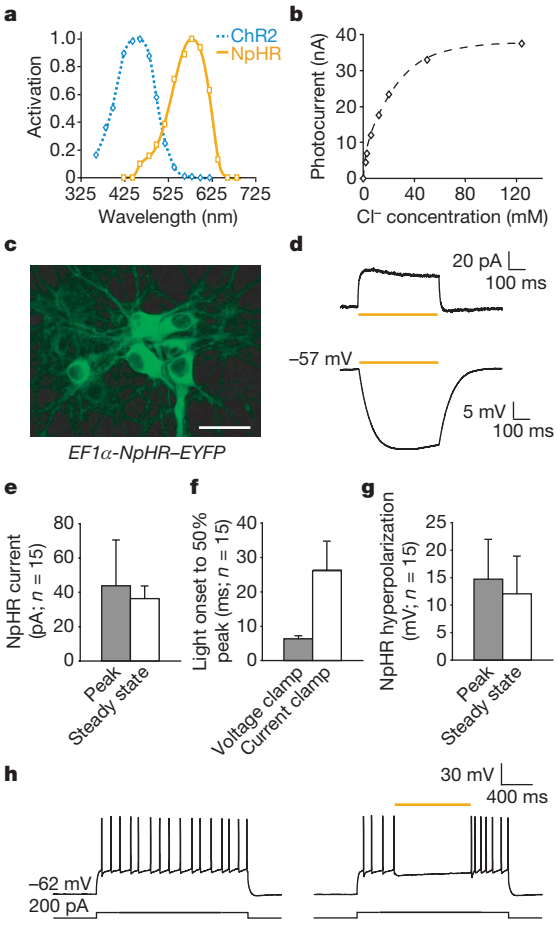

Figure 1 | Electrophysiological properties of NpHR in oocytes and hippocampal neurons. **a**, Action spectrum of NpHR in oocytes held at −50 mV, determined by 20 nm narrow bandwidth interference filters. The ChR2 action spectrum is provided for comparison[4]. **b**, Extracellular [Cl^-] dependence of NpHR pump currents indicates a simple Michaelis–Menten type saturation with a K_M of 16 mM (dashed fit curve). **c**, Hippocampal neurons expressing NpHR–EYFP (scale bar 50 μm). **d**, Yellow light (593 nm)-induced outward photocurrent in neurons (top panel, voltage clamp) and membrane hyperpolarization (bottom panel, current clamp); illumination duration is indicated by the yellow bar. **e**, NpHR peak versus steady-state current (mean ± s.d.; $n = 15$). **f**, Latency of NpHR activity measured from light onset to 50% of the peak current or hyperpolarization (mean ± s.d.; $n = 15$). **g**, NpHR peak versus steady-state membrane hyperpolarization (mean ± s.d.; $n = 15$). **h**, Illumination with yellow light potently inhibited neuronal firing.

Effects of NpHR on neuronal physiology

We conducted extensive controls to test whether heterologous expression of NpHR in neurons would alter the membrane properties or survival of neurons. Lentiviral expression of NpHR for at least 2 weeks did not alter neuronal resting potential (−53.1 ± 6.3 mV for $NpHR^+$ cells, −57.0 ± 4.8 mV for $NpHR^-$ cells, and −56.7 ± 5.7 mV for $NpHR^+$ cells exposed to yellow light for 10 min followed by a delay period of 1 day; Supplementary Fig. 2a, $n = 12$ each) or membrane resistance (114.5 ± 34.1 MΩ for $NpHR^+$ cells, 108.9 ± 20.1 MΩ for $NpHR^-$ cells, and 111.4 ± 23 MΩ for the light-exposed $NpHR^+$ cells; Supplementary Fig. 2b, $n = 12$ each). These electrical measurements indicate that NpHR had little basal electrical activity or passive current-shunting ability and did not compromise cell health. We also tested the dynamic electrical properties of neurons with and without NpHR. There was no significant difference in the number of spikes evoked by 500 ms of a 300-pA current injection (7.5 ± 2.8 for $NpHR^+$ neurons, 10.7 ± 7.9 for $NpHR^-$ neurons, and 9.3 ± 5.1 for the light-exposed $NpHR^+$ neurons; Supplementary Fig. 2c). Finally, we stained live $NpHR^+$ neurons (with and without light exposure) and $NpHR^-$ neurons with the membrane-impermeant DNA-binding dye propidium iodide to assess cell survival. NpHR expression did not affect the percentage of neurons that took up propidium iodide

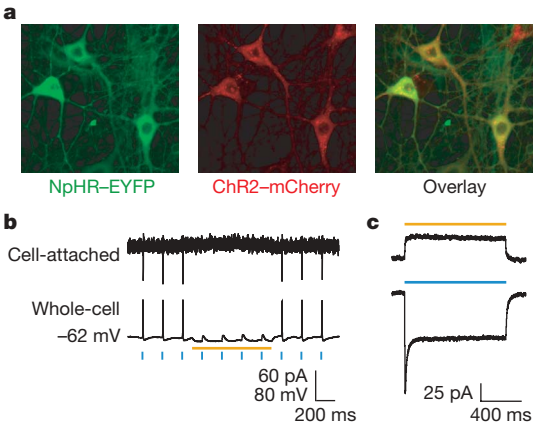

Figure 2 | Combining NpHR with ChR2 for noninvasive optical control. **a**, Hippocampal neurons co-expressing NpHR–EYFP under control of the *EF1α* promoter and ChR2–mCherry under control of the *synapsin I* promoter. **b**, Cell-attached and whole-cell recording of neurons co-expressing NpHR–EYFP and ChR2–mCherry. Action potentials are evoked by brief pulses of blue light (473 nm, 15 ms per pulse; length of blue bars is not to scale for ease of visualization). Simultaneous illumination with yellow light inhibited spike firing. **c**, Voltage-clamp recording from a single neuron co-expressing NpHR–EYFP and ChR2–mCherry, showing independently addressable outward and inward photocurrents in response to yellow and blue light, respectively.

(13/240 for NpHR$^+$ cells, 7/141 for NpHR$^-$ cells, and 10/205 for the light-exposed NpHR$^+$ cells; Supplementary Fig. 2d, $P > 0.999$ by χ^2 test). These experiments indicate that NpHR expression does not significantly affect the health or basal electrical properties of neurons.

NpHR operates over a range of timescales

To quantify the capabilities of NpHR for inhibiting neural activity, we first determined the tunability of NpHR efficacy with different intensities of delivered light. Using a 200 pA current step, which drove reliable action potential trains, we found that maximal light intensity of 21.7 mW mm^{-2} under a ×40, 0.8 numerical aperture water-immersion objective inhibited 98.2 ± 3.7% of the spikes (Fig. 3a and b). Using 33% or 50% of the full light intensity inhibited 74.9 ± 22.2% and 87.3 ± 13.5% of spikes, respectively (Fig. 3b). With steady current injection, lower intensities of light were effective for a shorter period of time; the delays from light onset to the first escaped spike under 33%, 50% and 100% light intensity were 533.65 ± 388.2 ms, 757.5 ± 235.5 ms and 990.5 ± 19.1 ms, respectively (Fig. 3c). Therefore, inhibition will be more effective early in the light pulse, presumably owing to the slight inactivation of NpHR. Except where otherwise noted, we conducted the rest of the experiments with 21.7 mW mm^{-2} yellow light delivered to the neurons.

Using trains of brief current pulses to generate spike trains, we tested whether NpHR could mediate both long-term inhibition (to emulate lesions on the timescale of seconds to minutes) and short-term inhibition (to modify spike firing on the millisecond timescale). We first tested long-term inhibition over 10 min by injecting 300-pA current pulses at 5 Hz to drive steady action potential firing. Concurrent yellow light was delivered continuously for 10 min. NpHR-mediated inhibition of spike trains was highly stable, remaining effective over many minutes (Fig. 3d). Almost all (99.0 ± 1.9%) spikes were inhibited within the first two minutes, and over 90% of spikes were inhibited for up to 8 min ($n = 5$; Fig. 3d, inset). The slight decrease in efficacy is probably due to accumulation of non-functional NpHRs with a deprotonated Schiff base over long periods of light exposure[24]. Although natural reprotonation of the Schiff base is slow, any non-functional NpHRs can be readily and quickly restored by brief illumination with blue light[24] (Supplementary Fig. 2h).

NpHR inhibits with single-spike precision

We next tested whether NpHR activation might allow the 'knockout' of single action potentials. Because the fast photocurrent of ChR2 enables brief pulses of blue light to drive reliable action potential trains[2], we used brief pulses of yellow light to test NpHR-mediated

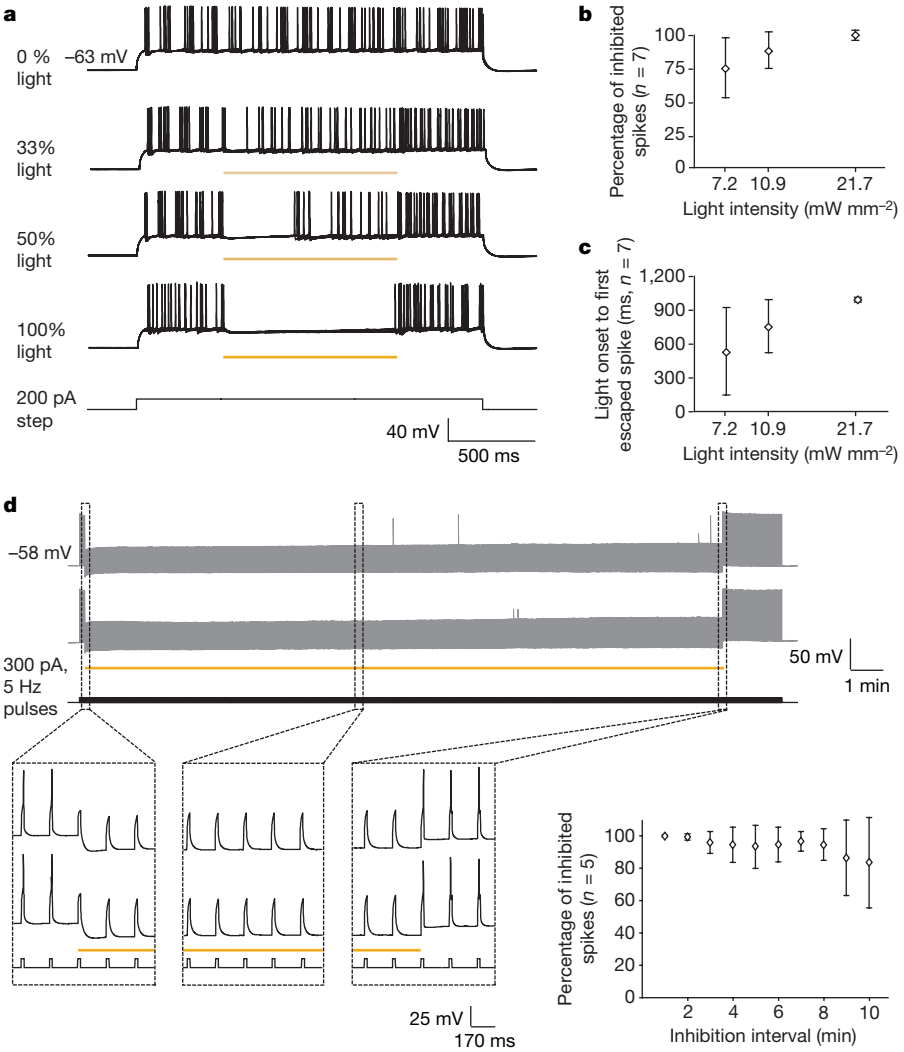

Figure 3 | NpHR mediates tunable neuronal inhibition over a range of timescales. **a**, Increasing intensities of light lead to stronger inhibition of spikes evoked by 200 pA of current injection (21.7 mW mm^{-2} at 100% intensity). **b**, Per cent of spikes inhibited at three different light intensities (1 s of light exposure, mean ± s.d.; $n = 7$). **c**, Duration of effective inhibition as measured by the delay from light onset to the first escaped spike (mean ± s.d.; $n = 7$). **d**, Ten min continuous illumination (two successive sweeps) robustly inhibited neuronal spike trains elicited by current pulse injection (300 pA, 5 Hz). Dashed boxes show the inhibition on an expanded timescale. Per cent efficacy of inhibition over 10 min measured by breaking down the 10 min interval into 1 min bins (inset, mean ± s.d.; $n = 5$).

inhibition. To assess the temporal resolution of spike inhibition, we attempted to inhibit pairs of spikes in action potential trains of 5, 10, 20 and 30 Hz (Fig. 4a) and found that single spikes could be reliably inhibited even from within spike trains (Fig. 4a). To define the temporal precision of NpHR we inhibited selected pairs of spikes with a range of inter-spike temporal delays. Both closely timed and temporally separated spike pairs could be reliably inhibited, while sparing spikes between the targeted times ($n = 6$, Fig. 4a–c). Over spike rates of 5 to 30 Hz, the closely timed spikes could be selectively inhibited with a probability of 0.95 or greater. We also found that by giving trains of millisecond-scale yellow light pulses, it was straightforward to simulate barrages of inhibitory postsynaptic potential (IPSP)-like events with precise, reliable timing and amplitudes, from 5 to 100 Hz (Fig. 4d). Because NpHR is a Cl^- pump and not a channel, the light-driven inhibition acts by shifting the membrane potential and will not contribute to shunting or input resistance changes. Indeed, we found that whereas the $GABA_A$ chloride channel agonist muscimol significantly decreased neuronal input resistance, NpHR activation had no detectable effect on the input resistance (Fig. 4e, f).

Because both ChR2 and NpHR can be activated with high temporal precision using millisecond-scale blue or yellow light pulses, we next asked if it would be possible to drive both proteins in intermingled, temporally precise patterns to non-invasively activate or inhibit single identified action potentials with light in the same experiment, or even in the same cell. Indeed, cell-attached and whole-cell recordings in hippocampal pyramidal neurons revealed that precisely patterned trains of yellow and blue light pulses can be used to evoke and inhibit neural activity with single-spike precision (Fig. 5a), and that NpHR can be used to override multiple preselected ChR2-driven spikes at identified positions in prolonged spike trains (Fig. 5a).

Application of NpHR in the mammalian brain

A crucial feature of ChR2 is that it can be functionally expressed in the mammalian brain without exogenous delivery of its required cofactor all-*trans*-retinal (ATR)[3], presumably owing to the presence of endogenous retinoids in the mammalian brain. We anticipated that this unique and important property could extend to NpHR, which also employs an ATR chromophore. To test this possibility, we delivered lentiviruses carrying NpHR–EYFP under the neuronal *CaMKIIα* promoter into the hippocampus of the adult mouse. Neurons throughout the hippocampus exhibited stable expression of NpHR–EYFP, as indicated by robust EYFP fluorescence (CA3 subfield shown; Fig. 5b, left

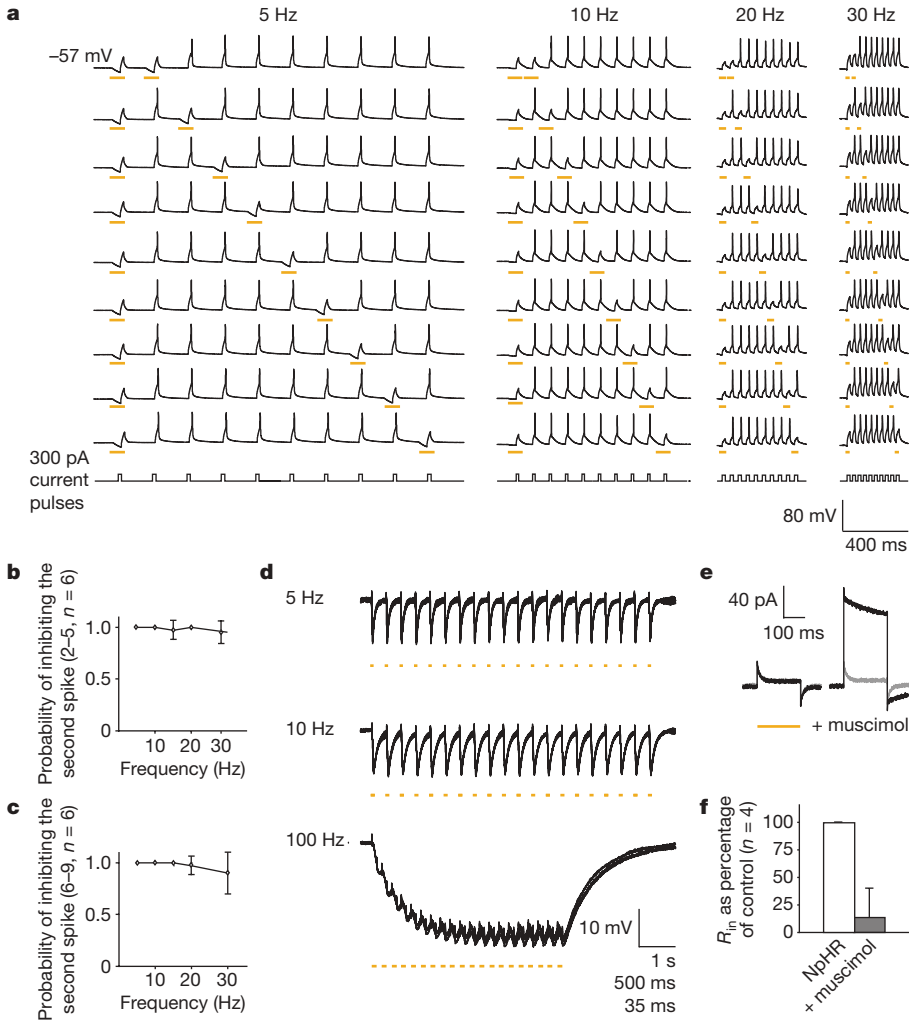

Figure 4 | Temporal precision of NpHR-mediated inhibition. **a**, Inhibition of spike pairs at different frequencies. Trains of ten spikes were evoked by 300 pA current injection pulses, and pairs of light pulses with variable temporal separation were used to inhibit the selected spikes. **b**, Probability of inhibiting the second spike in the pair, as a function of spike frequency, for short separations (spikes 2–5 in the spike train, mean ± s.d.; $n = 6$). **c**, Probability of inhibiting the second spike in the pair, as a function of spike frequency, for longer separations (spikes 6–9 in the spike train, mean ± s.d.; $n = 6$). **d**, NpHR can be employed to mimic precisely timed IPSP barrages at different frequencies; five successively acquired traces are overlaid for each frequency. **e**, Voltage-clamp recording of NpHR–EYFP-expressing neurons. Test pulses (5 mV, 200 ms) were used to test for changes in input resistance (R_{in}) during yellow light illumination or 50 nM muscimol application. Grey traces show the control condition. **f**, Summary plot showing that NpHR activation did not affect R_{in} (100.2 ± 1.15% of control, mean ± s.d.; $n = 4$), whereas muscimol application significantly decreased R_{in} (14 ± 26.8% of control, mean ± s.d.; $n = 4$).

panel). NpHR–EYFP cells in acute hippocampal slices exhibited voltage-clamp photocurrents similar to those observed in cultured neurons (data not shown), and current clamp recording of NpHR–EYFP neurons revealed that temporally precise patterns of spike inhibition could be achieved readily, as in dissociated culture (Fig. 5b, right panel). No exogenous cofactors were delivered at any point, indicating that NpHR can be functionally applied to mammalian systems *in vivo*.

Combining NpHR and ChR2 with imaging and behaviour

We next combined the NpHR/ChR2 system, expressed in living mammalian neural circuitry, with fura-2 calcium imaging in an all-optical experiment. Lentiviruses carrying ChR2–mCherry under the neuron-specific *CaMKIIα* promoter and NpHR–EYFP under the *EF1α* promoter were injected into the brain of postnatal day 4 (P4) mouse pups; acute cortical slices were prepared at P10–P14 and labelled with fura-2-acetoxymethyl. In neurons co-expressing ChR2–mCherry and NpHR–EYFP (Fig. 5c, left panel), initial simultaneous illumination with both blue and yellow light did not lead to intracellular calcium concentration ($[Ca^{2+}]_i$) transients, whereas subsequent pulsed blue light alone in the same neurons evoked ChR2-triggered $[Ca^{2+}]_i$ transients (Fig. 5c, middle panel), demonstrating that NpHR and ChR2 can be integrated to achieve multimodal, bidirectional control of neural activity in intact tissue. In the same imaged cells where ChR2 stimulation led to a $3.1 \pm 0.3\%$ increase in fluorescence intensity ratios $\Delta F/F_0$, the combination of NpHR and ChR2 activation resulted in a $0.0 \pm 0.2\%$ effect on $\Delta F/F$ ($n = 6$, $P < 0.0001$; Fig. 5c, right panel). Yellow illumination alone had no detectable effect on $[Ca^{2+}]_i$ (not shown). Because not all targeted cells are necessarily affected to the same degree (Fig. 1), this optical system could complement electrophysiology to probe successful modulation of the targeted cell population.

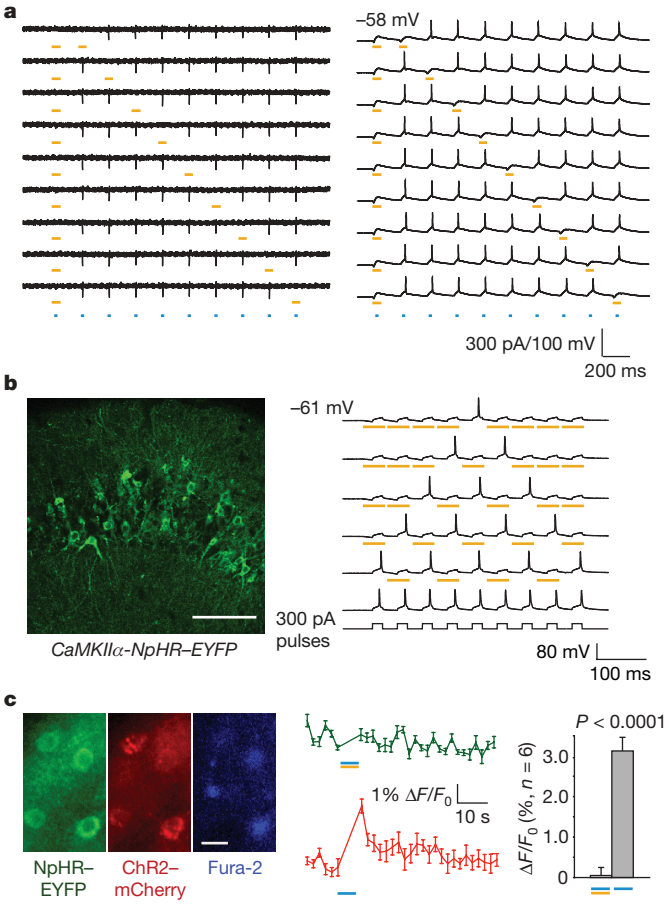

Figure 5 | Bidirectional optical neural control and *in vivo* implementation. **a**, Cell-attached (left panel) and whole-cell (right panel) recording of cultured hippocampal neurons co-expressing ChR–mCherry and NpHR–EYFP. Action potentials were evoked by trains of blue light pulses (5 Hz trains, 15 ms pulse width, blue bars). NpHR-mediated inhibition was co-administered by brief yellow light pulses (50 ms pulse width, yellow bars). **b**, Confocal image from an acute mouse brain slice showing membrane-localized NpHR–EYFP expression in the hippocampal CA3 subfield (left panel; scale bar, 150 μm). Current-clamp recording at right shows NpHR-mediated inhibition of specific spikes during a train of action potentials evoked by pulsed current injection (300 pA, 20 Hz). **c**, Left panel, epifluorescence images of cortical neurons triple-labelled with NpHR–EYFP, ChR2–mCherry and Fura-2. Scale bar, 20 μm. Middle panel, simultaneous illumination of cells co-expressing NpHR–EYFP and ChR2–mCherry with steady yellow (continuous illumination, 6 s) and pulsed blue light (50 pulses at 15 ms per flash, 10 Hz) prevented $[Ca^{2+}]_i$ transients (top trace, mean ± s.e.; $n = 6$). Subsequent photostimulation of the same cells with blue light pulses (50 pulses at 15 ms per flash, 10 Hz) evoked reliable $[Ca^{2+}]_i$ transients (bottom trace). Right panel, summary graph of photostimulation-induced fluorescence changes (mean ± s.e.; $n = 6$ ChR2-activated triple-labelled cells).

Combining ChR2 and NpHR with calcium imaging provides an all-optical system for interrogation of neural circuits. We next asked if this system could robustly control animal behaviour *in vivo*. We first expressed an NpHR–ECFP fusion protein in the body wall muscles of the nematode *Caenorhabditis elegans* using the muscle-specific myosin promoter (*Pmyo-3*). ECFP fluorescence could be readily observed throughout muscle cells and membranous muscle arm extensions (Fig. 6a and Supplementary Fig. 3a). Because nematode worms (unlike mammals) seem not to have sufficient levels of endogenous retinoids[6], transgenic animals expressing NpHR in muscle were grown in medium containing ATR. Whole-cell voltage-clamp recordings from dissected muscles indeed demonstrated light-evoked outward currents (265 ± 82 pA, $n = 9$; Fig. 6a). To test effects on muscle activity, swimming behaviour in liquid medium was analysed. Consistent with the photocurrents observed, photoactivation of NpHR immediately (within ~150 ms) and essentially completely arrested swimming behaviour (Fig. 6a, b and Supplementary Movie 1). As controls, we used transgenic animals raised in the absence of ATR, and wild-type animals raised with and without ATR. Importantly, robust paralysing effects of light were observed, but consistently only in transgenic animals raised in the presence of ATR. When muscle-expressing animals were illuminated for 1 s, they quickly returned to their natural swimming rate after light-stimulus termination (Fig. 6b). When NpHR was activated in muscle for 10 s (Fig. 6b), animals remained uncoordinated for prolonged periods (up to 40 s), before a full recovery became apparent and normal swimming commenced (Supplementary Fig. 3c).

We next targeted NpHR to a specific class of genetically defined neurons *in vivo*. We expressed NpHR–ECFP in cholinergic motor neurons using the vesicular acetylcholine transporter promoter (*Punc-17*)[25]. When illuminated for 1 or 10 s, respectively, these animals also strongly reduced or essentially stopped swimming behaviour (Fig. 6b and Supplementary Movie 2). These animals, in contrast to the muscle-targeted individuals, recovered to normal swimming behaviour immediately. This may indicate that neurons have more powerful Cl^- homeostasis mechanisms than muscles, though in all cases full recovery was observed, as expected from the lack of toxicity observed in mammalian neurons (Supplementary Fig. 2).

When illuminated on solid agar substrate, transgenic animals expressing NpHR either in muscle or in cholinergic motor neurons, exhibited rapid inhibition of movement and relaxed their bodies, resulting in overall elongation by up to 9% within ~600 ms of illumination (Fig. 6c and Supplementary Movies 3, 4 and 5). Finally, we found that ChR2 and NpHR could be driven simultaneously in *C. elegans* as well. With either muscle or targeted cholinergic neuron expression (using the *Pmyo-3* or *Punc-17* promoters, respectively), NpHR rapidly and reversibly counteracted the shortening behaviour observed with ChR2 alone (Fig. 6d and Supplementary Movies 6 and 7). These experiments demonstrate for the first time that acetylcholine release can be efficiently triggered from *C. elegans* motor neurons using

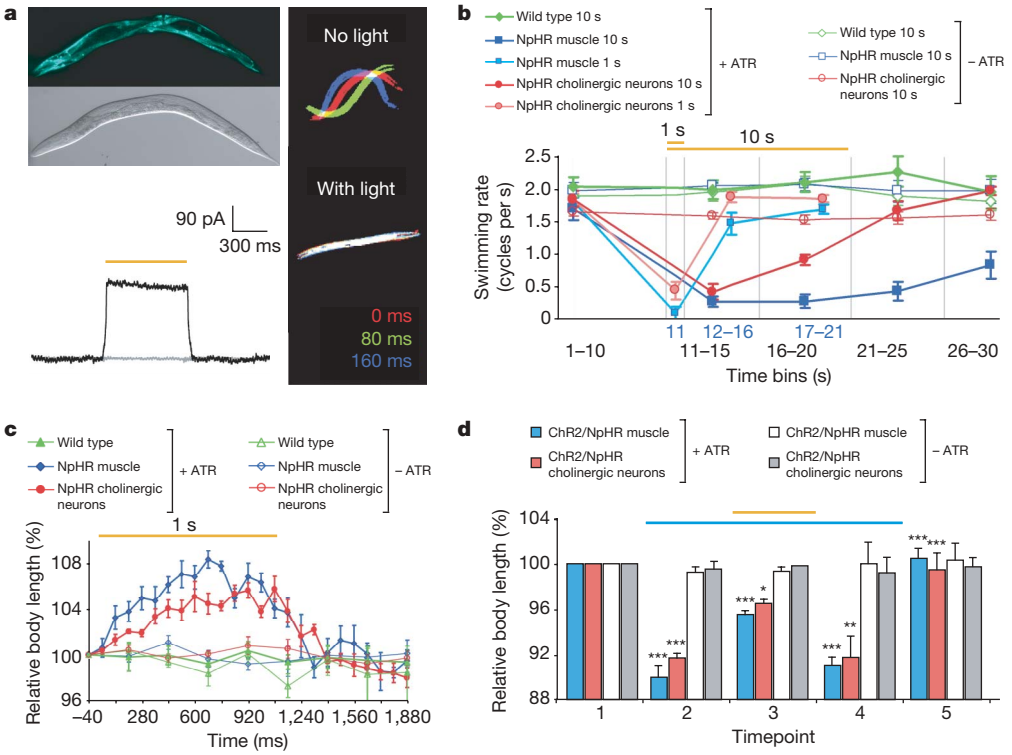

Figure 6 | Bidirectional optical control of *C. elegans*. **a**, Epifluorescence image showing *Pmyo-3*-mediated (transgene *zxEx30*) NpHR–ECFP expression in the body wall muscles of *C. elegans* (top left panels; see Supplementary Fig. 3a for higher magnification). Muscle voltage-clamp trace (bottom left panel) showing photocurrent in transgenic *C. elegans* expressing NpHR–ECFP (transgene *zxEx30*) and raised in the presence of ATR (black trace); note lack of response in transgenic animal raised in the absence of ATR (grey trace). NpHR activation targeted to muscle using *Pmyo-3* blocked swimming behaviour in liquid medium (right panels, transgene *zxEx29*). Animal postures from three consecutive movie frames (frame rate 12.5 Hz), either with or without NpHR photoactivation, were superimposed. **b**, Effect of 10 s illumination on swimming rate (mean ± s.e.; $n = 10$ for each set) in wild-type controls (green), animals expressing NpHR in muscles (transgene *zxEx29*; blue), or cholinergic motor neurons (transgene *zxEx33*; red). The number of swimming cycles per second was counted in bins of 10 s or 5 s intervals; illumination is shown as the orange bar. A briefer 1 s illumination protocol was also used, revealing rapid inhibition during illumination and faster recovery by comparison with the 10 s illumination (see also Supplementary Fig. 3c for full muscle recovery analysis). **c**, Effect of 1 s illumination on body length (mean ± s.e.; $n = 5$–6 for each set). Movies were taken from transgenic worms expressing NpHR in muscles (transgene *zxEx29*) or cholinergic motor neurons (transgene *zxEx33*). Plot shows the body length during the first frame before illumination, the 13 frames during the illumination, and the next 11 frames after illumination ended. Colour-coding and controls were as in **b**. **d**, Combined ChR2/NpHR expression in muscle cells (transgene *zxEx32*) or cholinergic motor neurons (transgene *zxEx34*) of worms. NpHR activation significantly reversed the muscle contraction caused by ChR2 activation (mean ± s.e.; $n = 6$ per condition; $^*P < 0.05$; $^{**}P < 0.01$; $^{***}P < 0.001$; between consecutive time points 1 s apart; *t*-test), but not in animals raised in the absence of ATR.

ChR2, and that ChR2 and NpHR work well together in nematodes as well as mammals.

Discussion

The NpHR/ChR2 system enables rapid bidirectional control of neurons on the timescale of milliseconds, thus enabling emulation or alteration of the neural code. These fast genetically based, neural-spike-controlling technologies powerfully augment existing tools for interrogating neural systems[26–33]. Although other optical neural modulators typically require the addition of exogenous chemicals[10,18,34,35], both NpHR and ChR2 can be functionally expressed and operate at high speed in the mammalian brain without necessitating cofactor addition. Moreover, NpHR and ChR2 function in *C. elegans* as well (Fig. 6) after simple dietary ATR supplementation[9]. When combined with imaging[36] or other measures in intact tissue or freely moving animals, the NpHR/ChR2 system provides the capability to directly and causally link precisely defined patterns of neural activity with specific circuit behaviours.

The ability to use light to inhibit[5,10,37] or activate[2,34,35,38–42] neurons may have practical applications beyond basic science investigation, as the NpHR/ChR2 system could be genetically targeted to specific classes of neurons or other excitable cells involved in disease processes to enable highly precise optical therapeutic treatments. For example, in Parkinson's disease electrode-based deep brain stimulation can be therapeutic for symptomatic relief but also gives rise to side effects. Delivery of these optogenetic tools targeted by cell-type-specific promoters to distinct disease-related neuronal types may provide a more precise alternative with fewer side effects and will lead to physiological insights into animal models of disease.

Whether applied in basic science or clinical applications, the spectral separation between the NpHR and ChR2 activation maxima permits both sufficiency and necessity testing in elucidation of the roles of specific cell types in high-speed intact circuit function. Indeed, integration of GFP-based probes and fura-2 with the NpHR/ChR2 neural control system delivers a powerful and complementary triad of technologies to identify, observe and control intact living neural circuitry with light.

METHODS SUMMARY

DNA constructs. Plasmid constructs were prepared according to standard molecular biology protocols. The lentiviral backbone was provided as a gift by P. Osten[43]. A list of *C. elegans* transgenes used can be found in Supplementary Table 1.

Lentivirus preparation and stereotactic injection. Lentiviruses were prepared as previously described[2] (a step-by-step instruction can be found in the methods). For electrophysiology, 1 µl of virus solution was injected into the hippocampal CA3 region of 5–7-week-old C57BL/6 mice (anteroposterior, −2.0 mm from bregma; lateral, 2 mm; ventral, 2.2 mm). For calcium imaging younger animals were used (postnatal day 4 or 5).

Electrophysiology and calcium imaging. Recordings in oocytes[4,20] and neurons[2] were carried out as previously described. Detailed composition of intra- and

extracellular solutions can be found in the methods. For calcium imaging, Fura-2-AM was loaded into the regions of interest as previously described[44]. Excitation of NpHR and ChR2 were accomplished using 593 nm and 437 nm excitation filters, respectively. The 300 W Lambda DG-4 (Sutter Instruments) was used for illumination and rapid wavelength switching. Frames were collected at 0.5 Hz. $[Ca^{2+}]_i$ changes were detected in single cells and expressed as the fluorescence intensity ratios $\Delta F/F_0$ with the resting fluorescence value F_0 determined at the beginning of each experiment. Patch clamping of *C. elegans* muscle was performed as previously described[6], at a holding potential of −40 mV.

***C. elegans* stimulation and electrophysiology.** Transgenic worms were generated using standard transgenic techniques. *C. elegans* were grown in the presence of ATR, as described previously[6] except that the ATR concentration was reduced to 5 μM. NpHR activation was achieved using a 50 W mercury lamp and band-pass filters. For co-activation of ChR2, a 473 nm laser was used.

Full Methods and any associated references are available in the online version of the paper at www.nature.com/nature.

Received 23 December 2006; accepted 14 March 2007.

1. Deisseroth, K. *et al.* Next-generation optical technologies for illuminating genetically targeted brain circuits. *J. Neurosci.* **26,** 10380–10386 (2006).
2. Boyden, E. S., Zhang, F., Bamberg, E., Nagel, G. & Deisseroth, K. Millisecond-timescale, genetically targeted optical control of neural activity. *Nature Neurosci.* **8,** 1263–1268 (2005).
3. Zhang, F., Wang, L. P., Boyden, E. S. & Deisseroth, K. Channelrhodopsin-2 and optical control of excitable cells. *Nature Methods* **3,** 785–792 (2006).
4. Nagel, G. *et al.* Channelrhodopsin-2, a directly light-gated cation-selective membrane channel. *Proc. Natl Acad. Sci. USA* **100,** 13940–13945 (2003).
5. Li, X. *et al.* Fast noninvasive activation and inhibition of neural and network activity by vertebrate rhodopsin and green algae channelrhodopsin. *Proc. Natl Acad. Sci. USA* **102,** 17816–17821 (2005).
6. Nagel, G. *et al.* Light activation of channelrhodopsin-2 in excitable cells of *Caenorhabditis elegans* triggers rapid behavioral responses. *Curr. Biol.* **15,** 2279–2284 (2005).
7. Ishizuka, T., Kakuda, M., Araki, R. & Yawo, H. Kinetic evaluation of photosensitivity in genetically engineered neurons expressing green algae light-gated channels. *Neurosci. Res.* **54,** 85–94 (2006).
8. Bi, A. *et al.* Ectopic expression of a microbial-type rhodopsin restores visual responses in mice with photoreceptor degeneration. *Neuron* **50,** 23–33 (2006).
9. Schroll, C. *et al.* Light-induced activation of distinct modulatory neurons triggers appetitive or aversive learning in *Drosophila* larvae. *Curr. Biol.* **16,** 1741–1747 (2006).
10. Banghart, M., Borges, K., Isacoff, E., Trauner, D. & Kramer, R. H. Light-activated ion channels for remote control of neuronal firing. *Nature Neurosci.* **7,** 1381–1386 (2004).
11. Ehrengruber, M. U. *et al.* Activation of heteromeric G protein-gated inward rectifier K^+ channels overexpressed by adenovirus gene transfer inhibits the excitability of hippocampal neurons. *Proc. Natl Acad. Sci. USA* **94,** 7070–7075 (1997).
12. Ibanez-Tallon, I. *et al.* Tethering naturally occurring peptide toxins for cell-autonomous modulation of ion channels and receptors *in vivo*. *Neuron* **43,** 305–311 (2004).
13. Isles, A. R. *et al.* Conditional ablation of neurones in transgenic mice. *J. Neurobiol.* **47,** 183–193 (2001).
14. Johns, D. C., Marx, R., Mains, R. E., O'Rourke, B. & Marban, E. Inducible genetic suppression of neuronal excitability. *J. Neurosci.* **19,** 1691–1697 (1999).
15. Kobayashi, K. *et al.* Targeted disruption of the tyrosine hydroxylase locus results in severe catecholamine depletion and perinatal lethality in mice. *J. Biol. Chem.* **270,** 27235–27243 (1995).
16. Lechner, H. A., Lein, E. S. & Callaway, E. M. A genetic method for selective and quickly reversible silencing of mammalian neurons. *J. Neurosci.* **22,** 5287–5290 (2002).
17. Nitabach, M. N., Blau, J. & Holmes, T. C. Electrical silencing of *Drosophila* pacemaker neurons stops the free-running circadian clock. *Cell* **109,** 485–495 (2002).
18. Tan, E. M. *et al.* Selective and quickly reversible inactivation of mammalian neurons *in vivo* using the *Drosophila* allatostatin receptor. *Neuron* **51,** 157–170 (2006).
19. Karpova, A. Y., Tervo, D. G., Gray, N. W. & Svoboda, K. Rapid and reversible chemical inactivation of synaptic transmission in genetically targeted neurons. *Neuron* **48,** 727–735 (2005).
20. Nagel, G. *et al.* Channelrhodopsin-1: a light-gated proton channel in green algae. *Science* **296,** 2395–2398 (2002).
21. Kolbe, M., Besir, H., Essen, L. O. & Oesterhelt, D. Structure of the light-driven chloride pump halorhodopsin at 1.8 Å resolution. *Science* **288,** 1390–1396 (2000).
22. Bamberg, E., Tittor, J. & Oesterhelt, D. Light-driven proton or chloride pumping by halorhodopsin. *Proc. Natl Acad. Sci. USA* **90,** 639–643 (1993).
23. Duschl, A., McCloskey, M. A. & Lanyi, J. K. Functional reconstitution of halorhodopsin. Properties of halorhodopsin-containing proteoliposomes. *J. Biol. Chem.* **263,** 17016–17022 (1988).
24. Hegemann, P., Oesterhelt, D. & Bamberg, E. The transport activity of the light-driven chloride pump halorhoposin is regulated by green and blue light. *Biochim. Biophys. Acta* **819,** 195–205 (1985).
25. Alfonso, A., Grundahl, K., Duerr, J. S., Han, H. P. & Rand, J. B. The *Caenorhabditis elegans unc-17* gene: a putative vesicular acetylcholine transporter. *Science* **261,** 617–619 (1993).
26. Faumont, S. & Lockery, S. R. The awake behaving worm: simultaneous imaging of neuronal activity and behavior in intact animals at millimeter scale. *J. Neurophysiol.* **95,** 1976–1981 (2006).
27. Rosenmund, C. *et al.* Differential control of vesicle priming and short-term plasticity by Munc13 isoforms. *Neuron* **33,** 411–424 (2002).
28. Yoon, H., Enquist, L. W. & Dulac, C. Olfactory inputs to hypothalamic neurons controlling reproduction and fertility. *Cell* **123,** 669–682 (2005).
29. Lu, J., Sherman, D., Devor, M. & Saper, C. B. A putative flip-flop switch for control of REM sleep. *Nature* **441,** 589–594 (2006).
30. Schoppa, N. E. & Westbrook, G. L. Glomerulus-specific synchronization of mitral cells in the olfactory bulb. *Neuron* **31,** 639–651 (2001).
31. Hanks, T. D., Ditterich, J. & Shadlen, M. N. Microstimulation of macaque area LIP affects decision-making in a motion discrimination task. *Nature Neurosci.* **9,** 682–689 (2006).
32. Kanold, P. O., Kara, P., Reid, R. C. & Shatz, C. J. Role of subplate neurons in functional maturation of visual cortical columns. *Science* **301,** 521–525 (2003).
33. Jensen, O. & Lisman, J. E. Novel lists of 7 ± 2 known items can be reliably stored in an oscillatory short-term memory network: interaction with long-term memory. *Learn. Mem.* **3,** 257–263 (1996).
34. Lima, S. Q. & Miesenbock, G. Remote control of behavior through genetically targeted photostimulation of neurons. *Cell* **121,** 141–152 (2005).
35. Shoham, S., O'Connor, D. H., Sarkisov, D. V. & Wang, S. S. Rapid neurotransmitter uncaging in spatially defined patterns. *Nature Methods* **2,** 837–843 (2005).
36. Helmchen, F., Fee, M. S., Tank, D. W. & Denk, W. A miniature head-mounted two-photon microscope. high-resolution brain imaging in freely moving animals. *Neuron* **31,** 903–912 (2001).
37. Pettit, D. L. & Augustine, G. J. Distribution of functional glutamate and GABA receptors on hippocampal pyramidal cells and interneurons. *J. Neurophysiol.* **84,** 28–38 (2000).
38. Volgraf, M. *et al.* Allosteric control of an ionotropic glutamate receptor with an optical switch. *Nature Chem. Biol.* **2,** 47–52 (2006).
39. Chambers, J. J., Banghart, M. R., Trauner, D. & Kramer, R. H. Light-induced depolarization of neurons using a modified Shaker K+ channel and a molecular photoswitch. J. Neurophysiol. **96,** 2792–2796 (2006).
40. Zemelman, B. V., Lee, G. A., Ng, M. & Miesenbock, G. Selective photostimulation of genetically chARGed neurons. *Neuron* **33,** 15–22 (2002).
41. Wang, S. S., Khiroug, L. & Augustine, G. J. Quantification of spread of cerebellar long-term depression with chemical two-photon uncaging of glutamate. *Proc. Natl Acad. Sci. USA* **97,** 8635–8640 (2000).
42. Adams, S. R. & Tsien, R. Y. Controlling cell chemistry with caged compounds. *Annu. Rev. Physiol.* **55,** 755–784 (1993).
43. Dittgen, T. *et al.* Lentivirus-based genetic manipulations of cortical neurons and their optical and electrophysiological monitoring *in vivo*. *Proc. Natl Acad. Sci. USA* **101,** 18206–18211 (2004).
44. MacLean, J. N., Fenstermaker, V., Watson, B. O. & Yuste, R. A visual thalamocortical slice. *Nature Methods* **3,** 129–134 (2006).

Supplementary Information is linked to the online version of the paper at www.nature.com/nature.

Acknowledgements We thank J. Huguenard for discussions; L. Meltzer and H.-C. Tsai for assistance with confocal imaging; R. Airan for statistical assistance; V. Gradinaru for help with calcium imaging; M. Engelhard, J. Rand, D. Oesterhelt, R. Abele, and B. Bauer for plasmids; and K. Zehl and E. Grabski for expert technical assistance. F.Z. is supported by a fellowship from the NIH. L.-P.W. is supported by a fellowship from the California Institute of Regenerative Medicine. F.Z. and L.-P.W. are co-first authors. E.B. and G.N. are supported by grants from the Max-Planck-Society and by the Deutsche Forschungsgemeinschaft. A.G. is supported by grants from the Hessisches Ministerium für Wissenschaft und Kunst, and by the Deutsche Forschungsgemeinschaft. K.D. is supported by NARSAD, APIRE and the Snyder, Culpeper, Coulter, Klingenstein, Whitehall, McKnight, and Albert Yu and Mary Bechmann Foundations, as well as by NIMH, NIDA, and the NIH Director's Pioneer Award Program.

Author Information The GenBank accession number is EF474018 for the 'mammalianized' NpHR sequence and EF474017 for the 'mammalianized' ChR2(1-315) sequence. Reprints and permissions information is available at www.nature.com/reprints. The authors declare no competing financial interests. Correspondence and requests for materials should be addressed to K.D. (deissero@stanford.edu).

METHODS

Oocyte microinjection and electrophysiology. NpHR complementary RNA was generated using the T7-cap scribe kit from Ambion. Stage V/VI oocytes were prepared as described elsewhere[45]. Each oocyte was injected with 30 to 50 ng cRNA, and incubated for 4 to 7 days at 16 to 18 °C with 1 μM ATR in the medium (90 mM NaCl, 2 mM KCl, 1 mM $MgCl_2$, 1.8 mM $CaCl_2$, 5 mM HEPES, pH 7.4/NaOH) to reconstitute functional halorhodopsins. As a control uninjected oocytes were incubated in the same medium. Oocytes were recorded using two-electrode voltage-clamp (Turbo Tec-05) and illuminated with a continuous He-Ne laser (594 nm, LYHR-0600M, Laser 2000). The maximum light intensity was 3 mW mm^{-2} and was focused to a diameter close to the dimensions of the oocyte. In giant patch experiments from halorhodopsin-expressing oocytes we used a continuous He-Ne laser of 633 nm with light intensities up to 400 mW mm^{-2}.

Lentiviral vector construction. Lentiviral vectors containing *Synapsin I-ChR2–mCherry*, *CaMKIIα-ChR2–mCherry*, and *CaMKIIα-NpHR–EYFP* were based on the FCK(1.3)GW plasmid (gift of P. Osten[43]). For the construction of these lentiviral vectors, the promoter was PCR amplified and cloned into the *Pac*I and *Age*I restriction sites. The transgene *ChR2–mCherry* or *NpHR–EYFP* were PCR amplified and cloned into the *Age*I and *Eco*RI restriction sites. The pLEHYT vector is constructed in the same way as pLECYT[2] by inserting the *NpHR–EYFP* gene into the *Afe*I and *Spe*I restriction sites of pLEGT (gift of E. Wexler and T. Palmer). For both *NpHR–EYFP* and *ChR2–mCherry*, the protein fusion was made using a *Not*I restriction site. The linker between the two proteins is 5′-GCGGCCGCC-3′. The start codon on the fluorescent protein was removed deliberately to avoid translation of the fluorescent protein alone. In addition to the promoter, each lentiviral vector contains the HIV-1 central polypurine tract (cPPT)[46] and the Woodchuck Hepatitis Virus Post-transcriptional Regulatory Element (WPRE)[47] to improve transduction efficiency.

Lentiviral production and transduction. High-titre lentiviruses were produced using a second generation lentiviral system, by co-transfection of 293FT cells (Invitrogen) with pCMVΔR8.74 and pMD2.G (both gifts of M. Sena-Esteves) in addition to the viral vector. A modified version of the protocol presented in Sena-Esteves *et al.*[48] was used. The protocol is reproduced below.

Day 0: Split 4 T-225 flasks (Nunc) of 95% confluent 293FT cells into 1 4-layer CellFactory (Nunc). Culture using 500 ml of DMEM with 10% FBS. Incubate the plates at 37 °C overnight. The cells should reach 90% confluence in 24 h.

Day 1: Perform calcium phosphate transfection. Make DNA mixture containing 690 μg of the viral vector, 690 μg of pCMVΔR8.74 and 460 μg of pMD2.G. Add 5.7 ml of 2 M $CaCl_2$ to the DNA mixture and bring the total volume to 23.75 ml with distilled H_2O. Then, quickly combine the DNA/$CaCl_2$ solution with 23.75 ml of 2× HBS (50 mM HEPES, 1.5 mM Na_2HPO_4, 180 mM NaCl, pH 7.05; note that the pH is important). After quickly mixing by inverting 5 times, add the DNA/$CaCl_2$/HBS solution to 500 ml of room-temperature DMEM with 10% FBS to make the transfection media. Then, exchange the media in the CellFactory with the transfection media.

Day 2: 15 h from the time of transfection, remove the transfection media from the CellFactory and wash the cells 3 times with fresh room-temperature DMEM. Incubation longer than 15 h may lead to cell death and reduced viral titre. Finally, replace the media with 500 ml of fresh DMEM containing 10% FBS and incubate in a 37 °C incubator for 9 h.

Day 2.5: 24 h from the time of transfection, remove the media from the CellFactory and replace with 200 ml of serum-free media (UltraCULTURE, Cambrex) containing 5 mM sodium butyrate. Return the CellFactory to the incubator.

Day 3: 40 h from the time of transfection, collect the 200 ml of media from the CellFactory. This is the viral-containing supernatant. Centrifuge at 1,000 r.p.m. for 5 min to precipitate large cell debris and then filter the viral supernatant using a 0.45 μm low-protein-binding filter flask. Then, centrifuge the supernatant using a SW-28 rotor (Beckman Coulter) for 2 h at 55,000*g* to precipitate the virus. Usually 6 centrifuge tubes are required to concentrate all of the viral supernatant. Before spinning, add 2 ml of PBS containing 20% sucrose to the bottom of the centrifuge tube to remove any remaining cell debris during centrifugation. After centrifugation, gently decant the liquid from the centrifuge tubes and resuspend all 6 viral pellets with 100 μl of 4 °C PBS. Then, aliquot the viral solution and store at −80 °C for future use. If desired, 10 ml of unconcentrated viral supernatant can be stored before centrifugation for *in vitro* use in cultured neurons. For culture applications, neurons can be transduced simply by adding 50 μl of unconcentrated viral supernatant per 24-well plate well. Protein expression can be observed 4 to 5 days later. For *in vivo* applications, concentrated virus can be directly injected into the mammalian brain as detailed below.

Stereotactic injection in the mouse brain. Female C57BL/6 mice, 5–7 weeks old, were housed according to the Laboratory Vertebrate Animals protocols at Stanford. The virus solution was delivered into the CA3 region of the hippocampus through stereotactic injection. Surgeries were performed under aseptic conditions. For anaesthesia, ketamine (16 mg kg^{-1} of body weight) and xylazine (5 mg kg^{-1} of body weight) cocktail were injected intraperitoneally. Fur was sheared from the top of the animal's head and the head was placed in a stereotactic apparatus (David Kopf Instruments). A midline scalp incision was made and a 1-mm-diameter craniotomy was drilled (anteroposterior, −2.0 mm from bregma; lateral, 2 mm; ventral, 2.2 mm). A glass micropipette was refilled with 3.0 μl of concentrated lentivirus solution using a programmable pump (PHD 2000, Harvard Apparatus) and 1 μl of lentivirus solution was injected at each site at a concentration of 0.1 μl min^{-1}.

Electrophysiology. Patch-clamp recordings in oocytes[4,20] and neurons[2] were carried out as previously described. For whole-cell and cell-attached recording in cultured hippocampal neurons or acute brain slices, three intracellular solutions containing chloride were prepared: 4 mM chloride (135 mM K-gluconate, 10 mM HEPES, 4 mM KCl, 4 mM MgATP, 0.3 mM Na_3GTP, titrated to pH 7.2); 10 mM chloride (129 mM K-gluconate, 10 mM HEPES, 10 mM KCl, 4 mM MgATP, 0.3 mM Na_3GTP, titrated to pH 7.2); or 25 mM chloride (114 mM K-gluconate, 10 mM HEPES, 25 mM KCl, 4 mM MgATP, 0.3 mM Na_3GTP, titrated to pH 7.2). For cultured hippocampal neurons, Tyrode's solution was employed as the extracellular solution (125 mM NaCl, 2 mM KCl, 3 mM $CaCl_2$, 1 mM $MgCl_2$, 30 mM glucose, and 25 mM HEPES, titrated to pH 7.3). For preparation of acute brain slices, mice were killed 2 weeks after viral injection. Acute brain slices (250 μm) were prepared in ice-cold cutting solution (64 mM NaCl, 25 mM NaHCO3, 10 mM glucose, 120 mM sucrose, 2.5 mM KCl, 1.25 mM NaH_2PO_4, 0.5 mM $CaCl_2$, 7 mM $MgCl_2$, and equilibrated with 95% O_2/5% CO_2) using a vibratome (VT1000S, Leica). Slices were incubated in oxygenated ACSF (124 mM NaCl, 3 mM KCl, 26 mM $NaHCO_3$, 1.25 mM NaH_2PO_4, 2.4 mM $CaCl_2$, 1.3 mM $MgCl_2$, 10 mM glucose, and equilibrated with 95% $+O_2$/5% CO_2) at 32 °C for 30 min to recover.

Fura-2-AM loading and Ca^{2+} imaging. For calcium imaging, lentiviruses were injected into the cortex of C57BL/6 mice at postnatal day 4 or 5 and acute brain slices were prepared 7 to 8 days later as described for adult mice. Fura-2-AM was loaded into the regions of interest as previously described[44]. Calcium activity was recorded on an upright fluorescence microscope (DM LFSA, Leica) with a ×20, 0.5 numerical aperture water immersion objective. The GFP/mRFP1 dual-bandpass dichroic (51022bs, Chroma) and emitter (51022m, Chroma) was used for both photostimulation and Ca^{2+} imaging. NpHR was excited using the 593/40 bandpass filter (FF01-593/40-25, Semrock) and ChR2 was excited using the 472/30 bandpass filter (FF01-472/30-25, Semrock). Simultaneous activation of NpHR and ChR2 was achieved using either the GFP/mRFP1 dual bandpass filter (51022x, Chroma) or the combination of a 473 nm blue diode laser (Crystal Lasers) and a 300 W Lambda DG-4 with a 593 nm excitation filter. Fura-2 was excited using the 340/26 bandpass filter (FF01-340/26-25, Semrock). Frames were collected using a cooled CCD camera (Retiga EXi, QImaging) at 0.5 Hz using MetaFluor (Molecular Devices). $[Ca^{2+}]_i$ changes were detected in single cells and expressed as the fluorescence intensity ratios $\Delta F/F_0$ with the resting fluorescence value F_0 determined at the beginning of each experiment.

Transgenic *C. elegans* lines and transgenes. The *NpHR* gene was placed under the muscle-specific *myo-3* promoter (untagged NpHR in transgene *zxEx29[pmyo-3-NpHR; lin-15$^+$]* and NpHR–ECFP in transgene *zxEx30[pmyo-3-NpHR –ECFP; rol-6d]*) or under the cholinergic motor neuron specific *unc-17* promoter (NpHR–ECFP in transgene *zxEx33[punc-17-NpHR –ECFP; lin-15$^+$]*). The NpHR–ECFP fusion (*zxEx30*, and *zxEx34*, see below) was employed to assess expression pattern. NpHR–ECFP (*zxEx30*) animals showed light-induced effects that were comparable to the untagged version (*zxEx29*).

For co-activation of ChR2/NpHR in muscles or cholinergic motor neurons, transgenes *zxEx32[pmyo-3-NpHR; pmyo-3-ChR2(H134R) –EYFP; lin-15$^+$]* and *zxEx34[punc-17-NpHR –ECFP; punc-17-ChR2(H134R)–YFP; rol-6d]* were used. A list of the transgenes and worm lines can be found in Supplementary Table 1.

***C. elegans* stimulation and electrophysiology.** *C. elegans* were grown in the presence of ATR, as described previously[6] except that the ATR concentration was reduced to 5 μM. For NpHR activation in behavioural assays, we used a Zeiss Axiovert 40 with a 50 W HBO mercury lamp, HQ-F41-007 excitation/emission filter set (excitation 530–560 nm, AHF Analysentechnik), or Zeiss Filterset 00 (excitation 530–585 nm), and either a 10× or 20× objective (10.2 and 4.4 mW mm^{-2}, respectively). For co-activation of ChR2, a blue DPSS laser (473 nm at 7 mW mm^{-2}, Pusch OptoTech) was used. Patch clamping of *C. elegans* muscle was performed as previously described[6], at a holding potential of −40 mV, using a Zeiss Axioskop 2 FS plus, equipped with a 100 W HBO mercury lamp, HQ-F41-007 filter set, and a ×40 water immersion objective (6.7 mW mm^{-2}).

45. Grygorczyk, R., Hanke-Baier, P., Schwarz, W. & Passow, H. Measurement of erythroid band 3 protein-mediated anion transport in mRNA-injected oocytes of *Xenopus laevis*. *Methods Enzymol.* **173,** 453–466 (1989).

46. Zennou, V. *et al.* The HIV-1 DNA flap stimulates HIV vector-mediated cell transduction in the brain. *Nature Biotechnol.* **19,** 446–450 (2001).
47. Brun, S., Faucon-Biguet, N. & Mallet, J. Optimization of transgene expression at the posttranscriptional level in neural cells: implications for gene therapy. *Mol. Ther.* **7,** 782–789 (2003).
48. Sena-Esteves, M., Tebbets, J. C., Steffens, S., Crombleholme, T. & Flake, A. W. Optimized large-scale production of high titre lentivirus vector pseudotypes. *J. Virol. Methods* **122,** 131–139 (2004).